aPKCi triggers basal extrusion of luminal mammary epithelial cells by tuning contractility and vinculin localization at cell junctions

Clémentine Villeneuve[a], Emilie Lagoutte[a], Ludmilla de Plater[b], Samuel Mathieu[a], Jean-Baptiste Manneville[a], Jean-Léon Maître[b], Philippe Chavrier[a], and Carine Rossé[a,1]

[a]Institut Curie, Paris Université Sciences et Lettres, Sorbonne Université, CNRS, UMR144, 75005 Paris, France; and [b]Institut Curie, Paris Université Sciences et Lettres, Sorbonne Université, CNRS UMR3215, INSERM U934, 75005 Paris, France

Edited by Peter Friedl, Radboud University Medical Center, Nijmegen, The Netherlands, and accepted by Editorial Board Member Anton Berns October 17, 2019 (received for review April 19, 2019)

Metastasis is the main cause of cancer-related deaths. How a single oncogenic cell evolves within highly organized epithelium is still unknown. Here, we found that the overexpression of the protein kinase atypical protein kinase C ι (aPKCi), an oncogene, triggers basally oriented epithelial cell extrusion in vivo as a potential mechanism for early breast tumor cell invasion. We found that cell segregation is the first step required for basal extrusion of luminal cells and identify aPKCi and vinculin as regulators of cell segregation. We propose that asymmetric vinculin levels at the junction between normal and aPKCi$^+$ cells trigger an increase in tension at these cell junctions. Moreover, we show that aPKCi$^+$ cells acquire promigratory features, including increased vinculin levels and vinculin dynamics at the cell–substratum contacts. Overall, this study shows that a balance between cell contractility and cell–cell adhesion is crucial for promoting basally oriented cell extrusion, a mechanism for early breast cancer cell invasion.

cell extrusion | vinculin | cell junction | atypical PKC ι | cell segregation

Most cancers in humans originate from mutations in epithelial cells. Tumorigenesis is a multistep process initiated from a single oncogenic cell in the epithelium (1, 2). Recent data suggest that metastatic dissemination can occur at an early stage during tumor formation. Certain cancer cells, particularly those in the breast, may spread before primary tumor detection and form metastases that can evolve independently and in parallel to the primary tumor (3, 4). The mechanisms responsible for the early escape of breast cancer cells from the epithelium are currently unknown.

Normal epithelial cells preserve the physiological barrier function of the epithelium and maintain tissue integrity by recognizing and actively eliminating aberrant or supernumerary cells through a mechanism called apical cell extrusion (5–8). This process is dependent on actomyosin contractility (9) and E-cadherin–mediated cell–cell adhesion (5, 10, 11). However, the overexpression of certain oncogenes, such as RasV12, has been shown to promote apical cell extrusion, although, importantly, RasV12 cells can also be basally extruded. Once basally extruded, these cancer cells, under the influence of survival factors, may be able to survive in the stroma (5, 10). Therefore, basally oriented cell extrusion may be a mechanism that allows transformed cells to escape from untransformed/normal epithelia (5, 10, 12, 13). How the apical versus basal direction of extrusion is controlled is yet to be elucidated. The asymmetric boundary between a transformed epithelial cell and surrounding normal counterparts is yet to be characterized, and its importance in cell extrusion is unknown.

Polarity proteins are often deregulated in cancers (14, 15). Loss of epithelial cell polarity is a hallmark of cancer cells that correlates with tumor aggressiveness. As polarity proteins are important for regulating cell–cell adhesion (16) and cell contractility (17), they may play essential roles in triggering cell extrusion and early tumor cell dissemination. Among them, the polarity protein kinase atypical protein kinase C ι (aPKCi) is an oncogene (18), of which the overexpression (aPKCi$^+$) is associated with a poor prognosis, in particular in breast cancer (19, 20).

Here, we show that aPKCi$^+$ cells are excluded from their normal counterparts in the breast luminal epithelial layer, suggesting that cell segregation is the first step for basal extrusion of aPKCi$^+$ luminal cells. We show an increase in cell tension at the interface between aPKCi$^+$ and wild-type (WT) cells dependent on myosin II activity, associated with a decrease of vinculin at the cell junctions. We identify aPKCi and vinculin as regulators of cell segregation and propose that a balance between cell contractility and cell–cell adhesion at the interface between normal and aPKCi$^+$ cells is crucial for promoting basally oriented epithelial cell extrusion in vivo. The decrease of vinculin at cell–cell junctions is concomitant with an increase in vinculin dynamics at focal adhesions in aPKCi$^+$ cells, which may contribute to the acquisition of promigratory features by these cells. In light of our results, we propose that basally oriented epithelial cell extrusion could be a mechanism underlying previously reported events of early breast cancer cell dissemination (3, 4).

Results and Discussion

We first investigated the effect of aPKCi overexpression in luminal epithelial cells in the mouse mammary gland in vivo. aPKCi was overexpressed in a limited number of mammary luminal cells to mimic the early steps of oncogenesis. We achieved limited

Significance

This study shows that an oncogenic mammary epithelial cell surrounded by normal cells can extrude basally in vivo and invade surrounding tissues without formation of a primary tumor. Here, we show that overexpression of the key polarity protein atypical protein kinase C ι (aPKCi) is sufficient for triggering basally oriented epithelial cell extrusion and early cell invasion into the mammary gland stroma. Moreover, we highlight the importance of the difference between the mechanical properties of aPKCi-overexpressing cells and those of the normal surrounding cells associated with the decrease of vinculin at the cell junction, which triggers cell segregation, the first step toward promoting and controlling the direction of cell extrusion.

Author contributions: C.R. designed research; C.V., E.L., L.d.P., and C.R. performed research; C.V., E.L., and J.-L.M. contributed new reagents/analytic tools; C.V., E.L., S.M., J.-B.M., J.-L.M., P.C., and C.R. analyzed data; and C.V., P.C., and C.R. wrote the paper.

The authors declare no competing interest.

This article is a PNAS Direct Submission. P.F. is a guest editor invited by the Editorial Board.

This open access article is distributed under Creative Commons Attribution-NonCommercial-NoDerivatives License 4.0 (CC BY-NC-ND).

[1]To whom correspondence may be addressed. Email: carine.rosse@curie.fr.

This article contains supporting information online at www.pnas.org/lookup/suppl/doi:10.1073/pnas.1906779116/-/DCSupplemental.

First published November 7, 2019.

expression by developing an in vivo assay in which mammary gland organoids from FVB mouse were virally transduced ex vivo with GFP, as a control (GFP^+), or GFP-aPKCi ($GFP\text{-}aPKCi^+$) at a suboptimal multiplicity of infection, and then grafted into the cleared mammary fat pad of a syngeneic animal (Fig. 1*A*). After 5 to 9 wk, grafted organoids successfully regenerated a mammary gland containing only a few GFP^+ or $GFP\text{-}aPKCi^+$ cells surrounded by WT luminal cells. We quantified GFP and $GFP\text{-}aPKCi^+$ epithelial cells negative for basal smooth muscle actin (SMA) or cytokeratin-5 markers and/or positive for cytokeratin-8 in the regenerated glands. Almost all GFP^+ epithelial cells were localized into the ducts, whereas 65% of $GFP\text{-}aPKCi^+$ cells were found outside the myoepithelial cell layer (Fig. 1 *B* and *C*) and 21% were also able to breach the basement membrane (BM) (Fig. 1 *D* and *E*). These data suggest that $GFP\text{-}aPKCi^+$ cells escaped from the duct and transmigrated through the myoepithelium and BM. Escaping $GFP\text{-}aPKCi^+$ cells were still positive for the luminal markers cytokeratin-8 and E-cadherin, suggesting that they have not undergone epithelial–mesenchymal transition (EMT) (Fig. 1 *B* and *D*). This result is similar to that of a previous study in which KRasV12 overexpression drove basal cell extrusion in pancreatic cancer cells without the involvement of classical EMT mechanisms (21). These results demonstrate that, in our in vivo model, which preserves a physiological microenvironment, aPKCi overexpression promotes basal extrusion of mammary luminal epithelial cells and cell invasion, without formation of a primary tumor.

We wanted to dissect the mechanisms involved in basally oriented epithelial cell extrusion. We thus turned to a simpler experimental setup based on a 3D mouse mammary organoid culture model (22, 23). We investigated the effect of aPKCi overexpression in a limited number of epithelial cells in mammary organoids imbedded in a 3D matrix of type I collagen and Matrigel. $GFP\text{-}aPKCi^+$ cells formed dynamic actin protrusions (*SI Appendix*, Fig. S1*A* and Movie S1) but retained features of polarized epithelial cells, such as subapical ZO-1 localization (*SI Appendix*, Fig. S1*B*). In addition, apoptotic markers were absent (*SI Appendix*, Fig. S1*C*), indicating that the extruding $GFP\text{-}aPKCi^+$ cells were alive. Forty-six percent of the $GFP\text{-}aPKCi^+$ luminal cells had breached the myoepithelial cell layer (SMA positive) versus 13% for the GFP^+ luminal cells (Fig. 2 *A* and *B*).

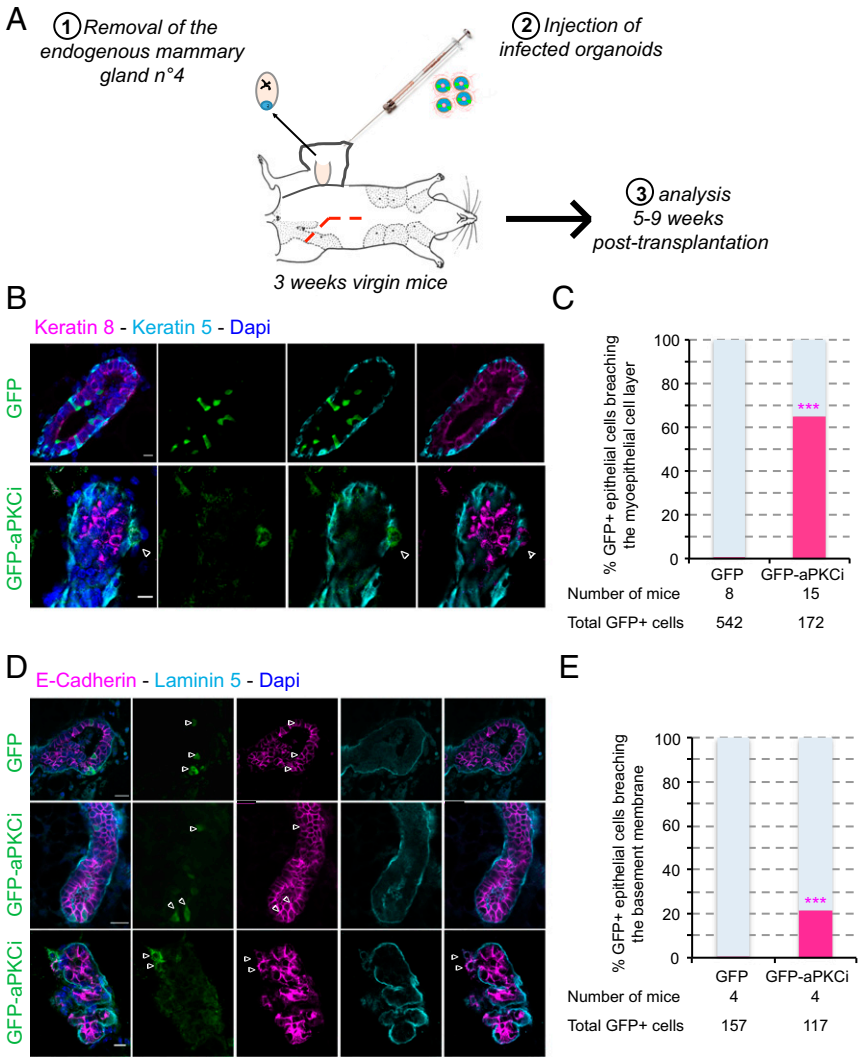

Fig. 1. aPKCi overexpression triggers basal extrusion of luminal cells in vivo. (*A*) Scheme of mouse mammary organoid transplantation experiments. (*B*) Confocal images of regenerated mammary glands from infected mouse organoids. Myoepithelial and luminal cells were stained with anti–cytokeratin-5 (cyan) and anti–cytokeratin-8 (magenta) antibodies, respectively. (*C*) Quantification of GFP^+ cells breaching the myoepithelial cell layer. A Fisher test was performed. (*D*) Confocal images of regenerated mammary glands from infected mouse organoids. The basement membrane (BM) and epithelial cells were stained with anti–laminin-5 (cyan) and anti–E-cadherin (magenta) antibodies, respectively. The white arrowheads show GFP-aPKCi cells escaping from the duct. (*E*) Quantification of GFP^+ cells breaching the BM. A Fisher test was performed. Nuclei were stained with DAPI (blue in *B* and *D*). (Scale bars, 10 μm.)

In addition, the BM continuity was interrupted in 33% of the cases (compared to none for GFP$^+$ luminal cells) (Fig. 2 *C* and *D*). We obtained similar results using mCherry-tagged constructs (*SI Appendix*, Fig. S2 *A* and *B*). In contrast to the transplantation experiments described above, complete basally oriented extrusion of GFP-aPKCi$^+$ luminal cells rarely occurred in the ex vivo model (8% of the cases compared to none for the GFP$^+$ cells). This may have been due to a reduced capacity of the organoid culture conditions to support the survival of isolated cells. However, the ex vivo organoid model recapitulates the in vivo situation, at least partially, and these data validate the mouse mammary organoid 3D culture system as an adequate model to study the first steps of basal extrusion of luminal epithelial cells in the mammary gland.

We then investigated the mechanisms involved in aPKCi-mediated BM breaching and cell extrusion. aPKCi controls the transport of membrane type I matrix metalloproteinase (MT1-MMP) to the surface, a key metalloproteinase for cell invasion (20). First, we tested the effect of MT1-MMP overexpression and observed that it had no effect on basal protrusion formation through the myoepithelial cell layer (*SI Appendix*, Fig. S2 *A* and *B*). However, there was a decreased number of aPKCi-dependent myoepithelium-breaching protrusions in the presence of GM6001, an inhibitor of MMP activity (*SI Appendix*, Fig. S2 *C* and *D*), suggesting that aPKCi-mediated protrusion formation is dependent on MMP activity. Additionally, we investigated whether overexpression of aPKCi can affect the apical polarity of the centrosome, as aPKC is known to control centrosome polarity (24). GFP$^+$ or GFP-aPKCi$^+$ cells were divided into 4 equal sectors (apical, basal, and 2 lateral sectors), and the number of centrosomes in each sector quantified by immunostaining using the centrosome marker, pericentrin. The centrosomes of 37% of GFP-aPKCi$^+$ epithelial cells were not located in the apical sector, compared to only 15% in control cells (*SI Appendix*, Fig. S3 *A* and *B*), suggesting aPKCi overexpression affects centrosome localization. In addition, inhibition of MMP activity by GM6001 (*SI Appendix*, Fig. S2 *C* and *D*) resulted in the centrosomes remaining polarized in the apical sector (*SI Appendix*, Fig. S3 *C* and *D*). These results suggest that changes in centrosome polarity are a consequence rather than a cause of basal protrusion formation (*SI Appendix*, Fig. S2 *C* and *D*). Basally extruded aPKCi-overexpressing cells, now in contact with the extracellular matrix, may engage receptors, such as integrins, which in turn may promote the reorientation of the centrosome at the front of the protrusive cell (24).

We next investigated whether GFP-aPKCi$^+$ cells segregate away from normal neighboring epithelial cells as an alternative mechanism. We thus set up a simpler model using immortalized nontransformed

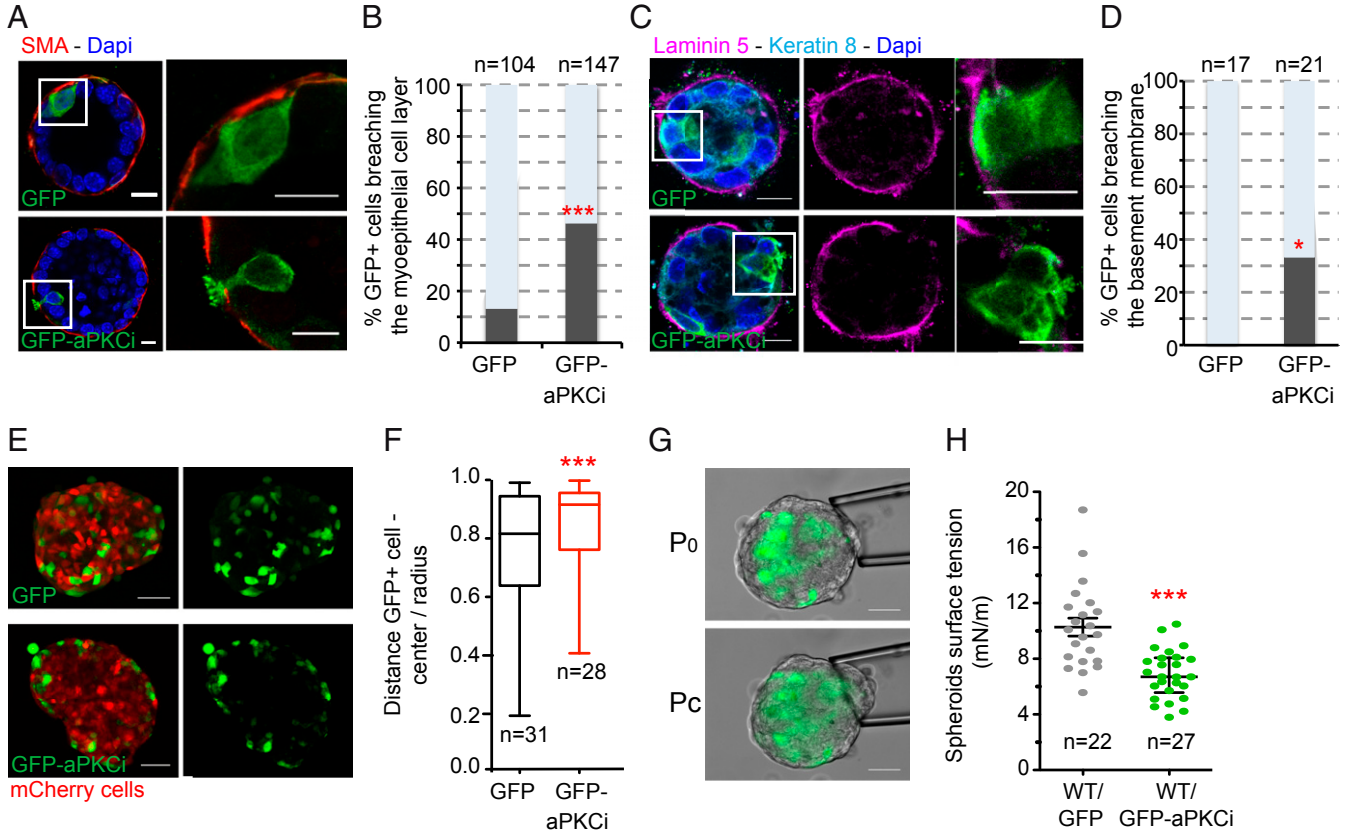

Fig. 2. aPKCi overexpression triggers basal epithelial cell protrusions breaching the BM and cell segregation from the MCF10A WT cell counterparts. (*A*) Confocal images of mouse mammary organoids with a few epithelial cells overexpressing GFP or GFP-aPKCi. Myoepithelial cells were detected with anti-SMA antibodies (red). Nuclei were stained with DAPI (blue). (*B*) Quantification of the total number of GFP$^+$ epithelial cells breaching the myoepithelial cell layer (***$P < 0.001$). Five independent experiments were performed. (*C*) Confocal images of mouse mammary organoids. Luminal cells and the BM are labeled with anti–cytokeratin-8 and anti–laminin-5 antibodies, respectively. (*D*) Quantification of the total number of GFP$^+$ epithelial cells breaching the BM (*$P < 0.05$). Two independent experiments were performed. Quantification of all GFP$^+$ cells was pooled from the independent experiments, and χ^2 tests were performed for all data. (Scale bars, 10 μm.) *n*, number of cells. (*E*) Confocal images of MCF-10A spheroids mixed with GFP$^+$ or GFP-aPKCi$^+$ cells and mCherry$^+$ cells. (Scale bars, 50 μm.) (*F*) Quantification of GFP$^+$ cell distribution. The graph shows the ratio between the distance of GFP$^+$ cells from the center of the spheroid and the radius of the spheroid (from 3 independent experiments). *n*, number of spheroids. A Mann–Whitney test was performed (***$P < 0.001$). (*G*) Images of micropipette aspiration of MCF-10A spheroids at the resting pressure P_0 (*Top*) and at the critical pressure P_c, for which the deformation of the spheroid reaches the micropipette radius (*Bottom*). (Scale bars, 50 μm.) (*H*) Individual (dots) and mean ± SEM (bars) surface tension measurements on spheroids containing a mix of WT and GFP$^+$ or GFP-aPKCi$^+$ cells. A Student *t* test was performed (***$P < 0.001$). Three independent experiments were performed. *n*, number of spheroids.

mammary epithelial MCF-10A cells. We validated this model by testing the effect of aPKCi overexpression in a subset of MCF-10A cells in polarized acini that formed when cells were cultured on top of Matrigel (25). We observed basal extrusion of GFP-aPKCi$^+$ luminal cells from the surrounding normal cells (*SI Appendix*, Fig. S4*A*), validating the use of the MCF-10A cell to dissect the mechanisms triggered by aPKCi overexpression. Then, we addressed whether GFP-aPKCi$^+$ epithelial cells can segregate from normal cells by adapting a 3D segregation assay described previously (26). Spheroids were generated by mixing MCF-10A cells overexpressing GFP-aPKCi with MCF-10A cells expressing mCherry in agarose. Agarose was used to avoid interference caused by cell adhesion to the substrate. GFP- aPKCi$^+$ cells segregated from mCherry-positive cells at the periphery of the spheroids (Fig. 2 *E* and *F* and *SI Appendix*, Fig. S4*B*). On the contrary, MCF-10A cells depleted of aPKCz/i preferentially localized to the center of the spheroids (*SI Appendix*, Fig. S4 *D* and *E*). These results show that the expression level of aPKCi in mammary epithelial cells controls their segregation from their normal counterparts. Previous studies have shown that cell segregation is driven by differences in cell surface tension (27). We examined whether aPKCi overexpression could affect the mechanical properties of the spheroids by measuring the surface tension of the spheroids at the cell–medium interface using the micropipette aspiration assay (28). The surface tension of the spheroids containing GFP-aPKCi$^+$ cells was one-half that of spheroids containing the same proportion of GFP$^+$ control cells (Fig. 2 *G* and *H*). Therefore, this increased surface tension of GFP-aPKCi$^+$ could be responsible for cell segregation.

Cell contractility and cell–cell adhesion are known to contribute to surface tension (29), as well as cell segregation (26) and cell extrusion (9, 10). For that reason, we impaired cell contractility and cell–cell adhesion in MCF-10A GFP$^+$ cells using small interfering RNA (siRNA) against RhoA or E-cadherin, respectively (*SI Appendix*, Fig. S4 *F–H*). Similarly to GFP-aPKCi$^+$ cells, cells with reduced contractility or adhesion were enriched at the periphery of the spheroids, confirming an important role for these 2 processes in cell segregation, as described in other models (26). We next investigated the effect of aPKCi overexpression on cell contractility to understand the mechanisms underlying the segregation and extrusion of GFP-aPKCi$^+$ cells. Although aPKCi overexpression had no effect on the overall expression of MLC2 or phospho-Ser19-MLC2 (*SI Appendix*, Fig. S5*A*), there was a large increase in actomyosin staining in apicolateral cell–cell junctions and in the protrusions of GFP-aPKCi$^+$ cells specifically when surrounded by their WT counterparts, both in MCF-10A monolayers (*SI Appendix*, Fig. S5 *B–D*) and mammary organoids (*SI Appendix*, Fig. S5*E*). Increased actomyosin density was specific to GFP-aPKCi$^+$ cells and was not observed in adjacent WT cells (*SI Appendix*, Fig. S5 *B* and *C* and Movie S2) or at the symmetrical interface between 2 GFP-aPKCi$^+$ cells (*SI Appendix*, Fig. S5 *F* and *G*). This result suggests that the surrounding normal epithelial cells may play an active role in the basally oriented extrusion of aPKCi-overexpressing cells, as proposed for the apical extrusion of oncogene-transformed cells (5, 30). We analyzed the tension at the junction between GFP-aPKCi$^+$ and WT cells (called asymmetric junctions) by laser ablation of individual junctions (*SI Appendix*, Fig. S5 *H* and *I* and Movie S3). Quantification of the initial recoil velocity of various cell vertices after ablation (31) suggested greater tension at the asymmetric GFP-aPKCi$^+$/WT cell–cell boundaries than at the symmetrical GFP$^+$/WT cell–cell junctions (*SI Appendix*, Fig. S5*J*). One possibility is that the increase in contractile force generated in GFP-aPKCi$^+$ cells surrounded by normal cells favors the active segregation and escape of GFP-aPKCi$^+$ cells from the normal epithelium. We assessed whether the greater tension at the junctions is required for cell extrusion by treating organoids with blebbistatin, an inhibitor of nonmuscle myosin II (32). Treatment of mouse mammary organoids with blebbistatin blocked the formation of basal protrusions in GFP-aPKCi$^+$ cells, suggesting that contractility is required for the formation of basal protrusions (*SI Appendix*, Fig. S5 *K* and *L*). Collectively, these findings show that the greater tension at the cellular junctions of asymmetric GFP-aPKCi$^+$/WT cell–cell boundaries is associated with apical enrichment of actomyosin in GFP-aPKCi$^+$ cells, as observed in apical cell extrusion (10), and may contribute to generate forces to allow the GFP-aPKCi$^+$ cell to extrude from the normal epithelium into the stroma.

Cells with reduced contractility segregate at the periphery of spheroids (*SI Appendix*, Fig. S4 *F–H* and ref. 26). Thus, the increase of contractility in GFP-aPKCi$^+$ cells surrounded by WT cells cannot explain the observed segregation of GFP-aPKCi$^+$ cells from their WT counterparts at the periphery of spheroids. Therefore, we investigated the effect of aPKCi overexpression on cell–cell adhesion and whether this could explain the segregation of GFP-aPKCi$^+$ cells from their WT counterparts. There was no significant change in the expression of the cell–cell adhesion proteins E-cadherin, α-catenin, or vinculin in MCF-10A GFP-aPKCi$^+$ cells (*SI Appendix*, Fig. S5*A*). The distribution of E-cadherin and α-catenin was normal at GFP-aPKCi$^+$/WT cell–cell junctions (Fig. 3 *A–C* and *SI Appendix*, Fig. S6*A*). Here, we cannot exclude that aPKCi overexpression in epithelial mammary cells might also control recycling of E-cadherin proteins to the cell surface to engage in cell–cell adhesion. In contrast to the apical cell extrusion process (5, 10, 11), little is known about whether a change in E-cadherin turnover at the junction could impact basally oriented cell extrusion and this aspect should be addressed in the future. Interestingly, vinculin staining was lower in both MCF-10A and primary mouse mammary luminal cells compared to other interfaces (Fig. 3 *A*, *D*, and *E* and *SI Appendix*, Fig. S6*B*). Vinculin is an α-catenin and F-actin–binding partner that localizes at cell–cell junctions and in focal adhesions that form cell–substratum contact sites (33). Vinculin is also known to be a tension sensor necessary for mechanosensing and force adaptation at adherens junctions; increased tension at junctions induces the reinforcement of vinculin (34, 35). Therefore, the observed decrease of vinculin in GFP-aPKCi$^+$/WT cell–cell junctions was unexpected, given the increase in contractility at these junctions (*SI Appendix*, Fig. S5). However, vinculin staining also decreased at the level of symmetric GFP-aPKCi$^+$/GFP-aPKCi$^+$ cell–cell junctions, in which E-cadherin localization was maintained (*SI Appendix*, Fig. S6 *C–E*). In addition, we did not also observe an increase in phospho-MLC2 at these symmetrical junctions (*SI Appendix*, Fig. S5 *B* and *C*). Vinculin could be a potential aPKCi substrate, as described for other PKCs (36), as the overexpression of aPKCi increased the phosphorylation of vinculin on serine residue(s) (*SI Appendix*, Fig. S6*F*). Phosphorylated vinculin may be unable to be recruited to cellular junctions independently of the level of tension at the cell junction. Overall, these data suggest that aPKCi may regulate vinculin phosphorylation in a cell-autonomous manner.

Vinculin is thought to stabilize cell–cell junctions through its interaction with α-catenin (37, 38). We thus investigated whether vinculin may have a role in cell segregation that could explain the effect of aPKCi overexpression on cell segregation. MCF-10A cells silenced for vinculin were mixed with WT cells in the 3D spheroid segregation assay (Fig. 2 *E* and *F* and *SI Appendix*, Fig. S4 *D* and *E*). Vinculin-depleted cells localized to the periphery of the spheroids when mixed with normal cells (Fig. 3 *F–H*), suggesting a role for vinculin in cell segregation. Consistent with this result, GFP-aPKCi$^+$ cells no longer segregated to the periphery of MCF10A cell spheroids when mixed with vinculin-depleted cells (Fig. 3 *I* and *J*). A possible explanation is that the decrease in vinculin recruitment at asymmetrical GFP-aPKCi$^+$/WT cell–cell junctions (Fig. 3 *C* and *D*) destabilizes the junctions, which in turn may favor the segregation of GFP-aPKCi$^+$ cells away from their normal neighbors. We assessed whether the increase in contractility and decrease in vinculin at GFP-aPKCi$^+$/WT cell junctions were linked by mixing MCF-10A cells silenced for vinculin with WT cells and observed a specific increase of phospho-MLC2 at the asymmetrical junctions between

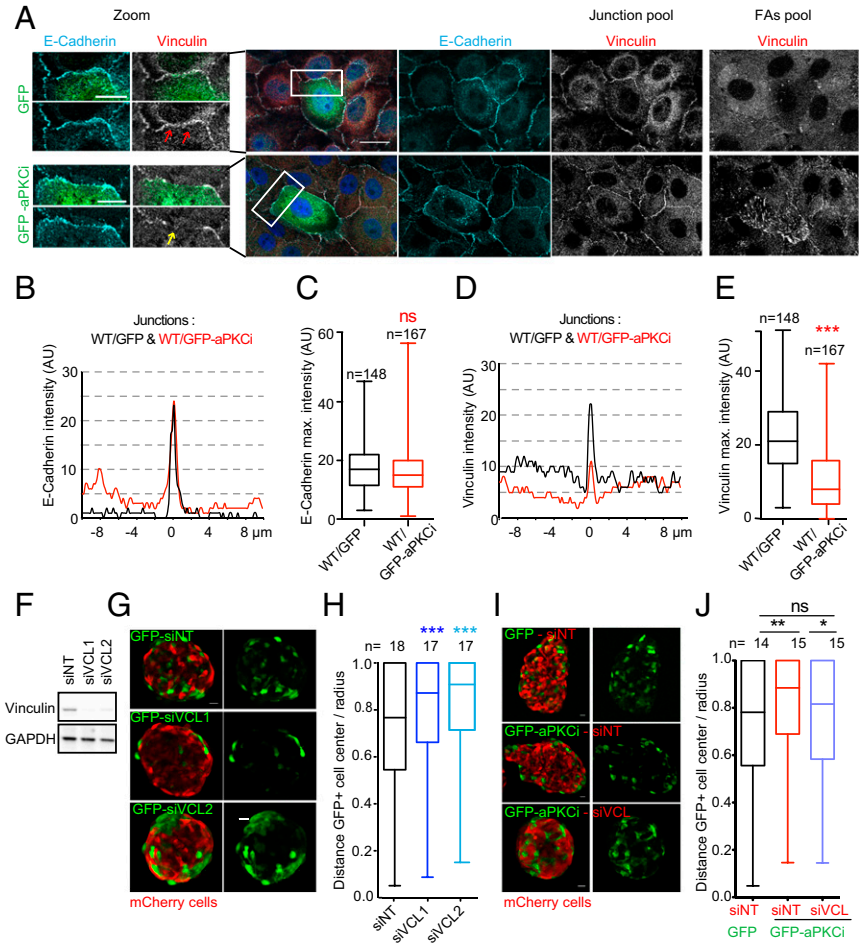

Fig. 3. A decrease of vinculin at junctions between WT and aPKCi$^+$ cells triggers the segregation of aPKCi$^+$ cells from normal cells. (*A*) Images of a monolayer of MCF-10A WT cells mixed with MCF-10A GFP or GFP-aPKCi cells on glass stained for nuclei (DAPI in blue), E-cadherin (cyan), and vinculin (red or gray). The *z* plane of focal adhesions (FAs) is 0.9 μm from the *z* plane of the junction (E-cadherin plane). (Scale bars, 20 μm and 10 μm for the zoom.) (*B*) Representative line scans of E-cadherin fluorescence intensity, in arbitrary units (AU), at the interface between a WT cell and a GFP$^+$ cell (black line) and between a WT cell and a GFP-aPKCi$^+$ cell (red line). (*C*) Quantification of the maximum intensity of E-cadherin staining at the interface between MCF-10A WT and GFP$^+$ cells or between MCF-10A WT and GFP-aPKCi$^+$ cells. A Mann–Whitney test was performed (ns, not significant). *n*, number of junctions. (*D*) Representative line scan of vinculin fluorescence intensity, in arbitrary units (AU), at the interface between a WT cell and a GFP$^+$ cell (black line) and between a WT cell and a GFP-aPKCi$^+$ cell (red line). (*E*) Quantification of the maximum intensity of vinculin staining at the interface between WT and GFP$^+$ cells or between MCF-10A WT and GFP-aPKCi$^+$ cells. A Mann–Whitney test was performed (***$P < 0.001$). *n*, number of boundaries. (*F*) Expression levels of vinculin in MCF-10A GFP cells treated with siNT, or 2 independent siVinculins (siVCLs). (*G*) Mixed spheroids of MCF-10A mCherry cells and MCF-10A GFP treated with the indicated siRNA. (*H*) Quantification of cell segregation between mCherry and GFP$^+$ cells from 3 independent experiments. A Kruskal–Wallis test was performed (***$P < 0.001$). (*I*) Spheroids of MCF-10A mCherry cells treated with the indicated siRNA were mixed with MCF-10A GFP$^+$ or GFP-aPKCi$^+$ cells. (*J*) Quantification of GFP$^+$ cell distribution. The graph represents the ratio between the distances of GFP$^+$ cells from the center of the spheroid and the radius of the spheroid in 3 independent experiments. The Mann–Whitney test was performed (*$P < 0.05$, **$P < 0.01$; ns, not significant). *n*, number of spheroids. (Scale bars, 20 μm.)

siVinculin and WT cells (*SI Appendix*, Fig. S7 *A* and *B*, white arrows) but not at the symmetrical junctions between vinculin-depleted cells (*SI Appendix*, Fig. S7*A*). Consistent with this result, mixing of vinculin-depleted WT cells with GFP-aPKCi–overexpressing cells abolished the increase of phospho-MLC2 at GFP-aPKCi$^+$/WT cell junctions (*SI Appendix*, Fig. S7 *C* and *D*). Overall, these results strongly suggest that the occurrence of an asymmetrical junction, in terms of aPKCi or vinculin levels, triggers an increase in contractility at the cell junction, driving epithelial basally oriented cell extrusion of the aPKCi$^+$ cell from the epithelium.

Concomitant to the decrease in vinculin levels at cell–cell junctions in aPKCi-overexpressing cells, we observed a striking reinforcement of vinculin at focal adhesions in the basal protrusions extending underneath WT cells in the MCF10A cell monolayer (Fig. 3*A* and Movies S4–S6). Moreover, live-cell imaging of cells overexpressing fluorescently tagged vinculin revealed that focal adhesions were more dynamic in GFP-aPKCi$^+$ cells than in control GFP$^+$ cells (Movies S5 and S6). Therefore, similarly to previous studies (20, 39), our results suggest that aPKCi overexpression may lead to the acquisition of migratory and invasive properties of mammary epithelial cells that extrude from the epithelium, facilitating invasion into the surrounding extracellular matrix. Our data suggest that vinculin may switch between cell junctions and focal adhesions in an aPKCi-dependent manner. To date, it is not known whether vinculin can shuttle between cell–cell junctions and focal adhesions (40). Vinculin shuttling from cell–cell junctions to focal adhesion sites may not only control cell extrusion, but also promote efficient collective tumor cell invasion by affecting the dynamics of focal adhesions (41–43).

This study reveals a role for aPKCi in driving cell segregation by affecting vinculin localization at cell–cell junctions, which in turn increases cortical tension at the interface between aPKCi-overexpressing cells and normal cells. Together, these effects may contribute to drive basal extrusion of aPKCi$^+$ cells into the

extracellular matrix. Moreover, aPKCi overexpression leads to the acquisition of promigratory features by reinforcing the localization and function of vinculin at focal adhesions. The reinforcement of vinculin at cell–matrix adhesion sites in combination with its depletion at cell–cell junctions may also contribute to cell extrusion. Our results identify aPKCi as a key regulator of cell contractility, similar to what has been reported in blastomeres of mouse preimplantation embryos (17), suggesting that mechanical properties of the tissue may control tumor cell invasion at the onset of tumor progression. A balance between increased contractility and decreased adhesiveness between normal and oncogenic cells, mediated by asymmetric vinculin levels at the junction, is required to drive the initial cell segregation and subsequent basally oriented cell extrusion events of the transformed cell from the normal epithelium. How an asymmetrical junction, in terms of vinculin levels, triggers an increase in contractility at cell junctions is yet to be elucidated. We show cell segregation to be the first step in the promotion of cell extrusion and that it may be important for controlling the direction of the extrusion. It will be crucial to explore whether the orientation of cell extrusion can be dictated by the nature of the oncogenes and the biophysical properties of cancer cells.

Materials and Methods

Antibodies and Dyes for Live Imaging. References are provided in *SI Appendix*, Table S1. Rabbit polyclonal antibody against laminin 5 (laminin 322) was kindly provided by Monique Aumailley, University of Cologne, Cologne, Germany.

DNA Constructs, Lentivirus Production, MCF10A Cell Culture and Acini, Transfection, and Stable Cell Lines. For DNA constructs, lentivirus production, cell culture, transfection, and stable cell lines, see *SI Appendix, SI Experimental Procedures*.

Immunostaining of MCF-10A Cell Monolayers on Glass Coverslips and MCF10A Acini. See *SI Appendix, SI Experimental Procedures*.

Segregation Assays. MCF-10A spheroids were grown in 96-well plates coated with 50 μL of 1.5% low–melting-point agarose (#16520-050; Invitrogen). A drop of 100 μL of a heterogeneous population of MCF-10A cells (mCherry/GFP or mCherry/GFP-aPKCi at a ratio of 5:1) was deposited at a concentration of 10,000 cells per mL. Spheroids were grown for 20 h in MCF-10A medium.

Micropipette Experiments. MCF-10A spheroids were assembled as for segregation assays. Each spheroid was composed of an equal mix of WT/GFP or WT/GFP-aPKCi cells. Spheroids were placed in suspension in a nonadhesive glass-bottom culture dish and incubated at 37 °C and 5% CO_2 for microaspiration. The microaspiration setup (28) was built on an inverted Leica microscope equipped with an Eppendorf Transferman micromanipulator holding micropipettes connected to a Fluigent MFCS EZ microfluidic pump. Images were acquired with a 40×/0.8 numerical aperture dry objective. The surface tension at the cell–medium interface (γ_{cm}) of spheroids was measured as previously described (28). Surface tension was calculated using Laplace's law:

$$\gamma_{cm} = \frac{P_c}{2\left(\frac{1}{R_p} - \frac{1}{R_c}\right)},$$

in which R_c is the resting radius of curvature of the spheroid at the location of the measurement, and P_c is the critical pressure at which spheroid deformation reaches R_p, the micropipette radius. Shape analysis was performed using ImageJ and FIJI (44).

Mouse Strains. FVB mice from Charles River Laboratories were used in this study. The cytokeratin-14:Actin-GFP transgenic line was a gift from Elaine Fuchs, The Rockefeller University, New York, NY. The cytokeratin-14-GFP-actin transgene construct containing the human cytokeratin-14 promoter, rabbit β-globin intron, and EGFP-actin cDNA was randomly inserted into FVB mice. The mice express EGFP-tagged murine β-actin under the control of the cytokeratin-14 promoter, as previously described (45).

Isolation, Infection, and 3D Culture and Immunostaining of Primary Mammary Epithelial Organoids Cultivated in a 3D Matrix. For isolation, infection, and 3D culture and immunostaining of primary mammary epithelial organoids cultivated in a 3D matrix, see *SI Appendix, SI Experimental Procedures*.

In Vivo Transplantation Experiment and Tissue Immunofluorescence. Isolated mammary epithelial organoids from adult mammary tissues were infected as described above and directly transplanted into the inguinal fat pads, which had been cleared of endogenous epithelium as previously described (46, 47), of 3-wk-old FVB females (Charles River) of the same genetic background (syngeneic transplantation). Control and GFP-aPKCi organoids were developed in the identical hormonal context by colaterally injecting control and mutant mammary fragments into the fat-pad cushions of the same recipient mouse. Thus, the interindividual variability linked to the hormonal cycle was minimized, reducing the number of required animals. Primary outgrowths were collected after 5 to 9 wk and stained as described below. For tissue immunofluorescence, see *SI Appendix, SI Experimental Procedures*.

Microscopy, Laser Ablation, and Image Analysis. For microscopy, laser ablation, and image analysis, see *SI Appendix, SI Experimental Procedures*.

Immunoprecipitation Assay. For immunoprecipitation assay, see *SI Appendix, SI Experimental Procedures*.

Statistical Analysis. For statistical analysis, see *SI Appendix, SI Experimental Procedures*.

Ethics Approval. Animal care and use for this study were performed in accordance with the recommendations of the European Community (2010/63/UE) for the care and use of laboratory animals. Experimental procedures were specifically approved by the ethics committee of the Institut Curie CEEA-IC #118 (CEEA-IC 2017-013) in compliance with international guidelines.

ACKNOWLEDGMENTS. The authors acknowledge the Nikon Imaging Center at the Institut Curie–CNRS, Plateforme d'Imagerie Cellulaire et Tissulaire BioImaging de l'Institut Curie (member of the France-BioImaging national research infrastructure) for the fluorescence microscopy equipment and help with image acquisition. We are particularly grateful to the personnel of the Animal Facility and the Flow Cytometry Core Facility of Institut Curie. We thank Bethan Lloyd-Lewis (UMR3215/U934, Institut Curie) for comments on the manuscript, Marie-Ange Deugnier (UMR144, Institut Curie) for advice on mouse transplantation experiments, and Denis Krinja (UMR144, Institut Curie) for help with tissue immunostaining. The members of P.C.'s laboratory are thanked for helpful discussions. Funding for this work was provided by grants to C.R. from the Projet Fondation ARC pour la Recherche contre le Cancer (PJA20141201972 and PJA20181208073), Cancerôpôle Ile de France (EMERG-1, INVADOID 2016), and Groupement de l'Entreprise Française de Lutte contre le Cancer, Laboratory of Excellence (LABEX) CellPhyBio ANR-11-LABX-0038; and by core funding from Institut Curie and CNRS (to P.C.). C.V. is funded by a grant from Paris Sciences et Lettres (PSL) and Fondation pour la Recherche Médicale. S.M. is funded by a grant from the Sorbonne Université, Pierre and Marie Curie University Paris 06 (Programme Doctoral "Interfaces Pour le Vivant"). Research in the laboratory of J.-L.M., who is supported by Institut Curie, CNRS, and INSERM, is funded by the Action Thématique Incitative sur Programme-Avenir Program, a PSL "Nouvelle Équipe" grant, and LABEX DEEP (ANR-11-LBX-0044), which are part of Initiatives for Excellence PSL (ANR-10-IDEX-0001-02 PSL).

1. P. C. Nowell, The clonal evolution of tumor cell populations. *Science* **194**, 23–28 (1976).
2. D. Hanahan, R. A. Weinberg, Hallmarks of cancer: The next generation. *Cell* **144**, 646–674 (2011).
3. K. L. Harper *et al.*, Mechanism of early dissemination and metastasis in Her2$^+$ mammary cancer. *Nature* **540**, 588–592 (2016).
4. H. Hosseini *et al.*, Early dissemination seeds metastasis in breast cancer. *Nature* **540**, 552–558 (2016).
5. C. Hogan *et al.*, Characterization of the interface between normal and transformed epithelial cells. *Nat. Cell Biol.* **11**, 460–467 (2009).
6. G. T. Eisenhoffer *et al.*, Crowding induces live cell extrusion to maintain homeostatic cell numbers in epithelia. *Nature* **484**, 546–549 (2012).
7. S. A. Gudipaty, J. Rosenblatt, Epithelial cell extrusion: Pathways and pathologies. *Semin. Cell Dev. Biol.* **67**, 132–140 (2017).
8. T. B. Saw *et al.*, Topological defects in epithelia govern cell death and extrusion. *Nature* **544**, 212–216 (2017).
9. J. Rosenblatt, M. C. Raff, L. P. Cramer, An epithelial cell destined for apoptosis signals its neighbors to extrude it by an actin- and myosin-dependent mechanism. *Curr. Biol.* **11**, 1847–1857 (2001).
10. S. K. Wu, A. K. Lagendijk, B. M. Hogan, G. A. Gomez, A. S. Yap, Active contractility at E-cadherin junctions and its implications for cell extrusion in cancer. *Cell Cycle* **14**, 315–322 (2015).
11. S. K. Wu, S. Budnar, A. S. Yap, G. A. Gomez, Pulsatile contractility of actomyosin networks organizes the cellular cortex at lateral cadherin junctions. *Eur. J. Cell Biol.* **93**, 396–404 (2014).
12. C. T. Leung, J. S. Brugge, Outgrowth of single oncogene-expressing cells from suppressive epithelial environments. *Nature* **482**, 410–413 (2012).

13. G. M. Slattum, J. Rosenblatt, Tumour cell invasion: An emerging role for basal epithelial cell extrusion. *Nat. Rev. Cancer* **14**, 495–501 (2014).
14. B. Xue, K. Krishnamurthy, D. C. Allred, S. K. Muthuswamy, Loss of Par3 promotes breast cancer metastasis by compromising cell-cell cohesion. *Nat. Cell Biol.* **15**, 189–200 (2013).
15. L. M. McCaffrey, J. Montalbano, C. Mihai, I. G. Macara, Loss of the Par3 polarity protein promotes breast tumorigenesis and metastasis. *Cancer Cell* **22**, 601–614 (2012).
16. P. Coopman, A. Djiane, Adherens junction and E-Cadherin complex regulation by epithelial polarity. *Cell. Mol. Life Sci.* **73**, 3535–3553 (2016).
17. J. L. Maître *et al*., Asymmetric division of contractile domains couples cell positioning and fate specification. *Nature* **536**, 344–348 (2016).
18. A. P. Fields, R. P. Regala, Protein kinase C iota: Human oncogene, prognostic marker and therapeutic target. *Pharmacol. Res.* **55**, 487–497 (2007).
19. K. D. Awadelkarim *et al*., Quantification of PKC family genes in sporadic breast cancer by qRT-PCR: Evidence that PKCι/λ overexpression is an independent prognostic factor. *Int. J. Cancer* **131**, 2852–2862 (2012).
20. C. Rossé *et al*., Control of MT1-MMP transport by atypical PKC during breast-cancer progression. *Proc. Natl. Acad. Sci. U.S.A.* **111**, E1872–E1879 (2014).
21. Y. Gu *et al*., Defective apical extrusion signaling contributes to aggressive tumor hallmarks. *eLife* **4**, e04069 (2015).
22. K. V. Nguyen-Ngoc *et al*., ECM microenvironment regulates collective migration and local dissemination in normal and malignant mammary epithelium. *Proc. Natl. Acad. Sci. U.S.A.* **109**, E2595–E2604 (2012).
23. K. V. Nguyen-Ngoc *et al*., 3D culture assays of murine mammary branching morphogenesis and epithelial invasion. *Methods Mol. Biol.* **1189**, 135–162 (2015).
24. S. Etienne-Manneville, A. Hall, Integrin-mediated activation of Cdc42 controls cell polarity in migrating astrocytes through PKCzeta. *Cell* **106**, 489–498 (2001).
25. J. Debnath *et al*., The role of apoptosis in creating and maintaining luminal space within normal and oncogene-expressing mammary acini. *Cell* **111**, 29–40 (2002).
26. A. E. Cerchiari *et al*., A strategy for tissue self-organization that is robust to cellular heterogeneity and plasticity. *Proc. Natl. Acad. Sci. U.S.A.* **112**, 2287–2292 (2015).
27. M. Krieg *et al*., Tensile forces govern germ-layer organization in zebrafish. *Nat. Cell Biol.* **10**, 429–436 (2008).
28. K. Guevorkian, J. L. Maître, Micropipette aspiration: A unique tool for exploring cell and tissue mechanics in vivo. *Methods Cell Biol.* **139**, 187–201 (2017).
29. C. P. Heisenberg, Y. Bellaïche, Forces in tissue morphogenesis and patterning. *Cell* **153**, 948–962 (2013).
30. M. Kajita *et al*., Filamin acts as a key regulator in epithelial defence against transformed cells. *Nat. Commun.* **5**, 4428 (2014).
31. X. Liang, M. Michael, G. A. Gomez, Measurement of mechanical tension at cell-cell junctions using two-photon laser ablation. *Bio Protoc.* **6**, e2068 (2016).
32. A. F. Straight *et al*., Dissecting temporal and spatial control of cytokinesis with a myosin II inhibitor. *Science* **299**, 1743–1747 (2003).
33. E. E. Weiss, M. Kroemker, A. H. Rüdiger, B. M. Jockusch, M. Rüdiger, Vinculin is part of the cadherin-catenin junctional complex: Complex formation between alpha-catenin and vinculin. *J. Cell Biol.* **141**, 755–764 (1998).
34. Q. le Duc *et al*., Vinculin potentiates E-cadherin mechanosensing and is recruited to actin-anchored sites within adherens junctions in a myosin II-dependent manner. *J. Cell Biol.* **189**, 1107–1115 (2010).
35. S. Huveneers *et al*., Vinculin associates with endothelial VE-cadherin junctions to control force-dependent remodeling. *J. Cell Biol.* **196**, 641–652 (2012).
36. M. Perez-Moreno, A. Avila, S. Islas, S. Sanchez, L. González-Mariscal, Vinculin but not alpha-actinin is a target of PKC phosphorylation during junctional assembly induced by calcium. *J. Cell Sci.* **111**, 3563–3571 (1998).
37. S. Dufour, R. M. Mège, J. P. Thiery, α-Catenin, vinculin, and F-actin in strengthening E-cadherin cell-cell adhesions and mechanosensing. *Cell Adhes. Migr.* **7**, 345–350 (2013).
38. R. Seddiki *et al*., Force-dependent binding of vinculin to α-catenin regulates cell-cell contact stability and collective cell behavior. *Mol. Biol. Cell* **29**, 380–388 (2018).
39. C. Rosse *et al*., An aPKC-exocyst complex controls paxillin phosphorylation and migration through localised JNK1 activation. *PLoS Biol.* **7**, e1000235 (2009).
40. B. Noethel *et al*., Transition of responsive mechanosensitive elements from focal adhesions to adherens junctions on epithelial differentiation. *Mol. Biol. Cell* **29**, 2317–2325 (2018).
41. B. Ladoux, R. M. Mège, Mechanobiology of collective cell behaviours. *Nat. Rev. Mol. Cell Biol.* **18**, 743–757 (2017).
42. B. D. Hoffman, The detection and role of molecular tension in focal adhesion dynamics. *Prog. Mol. Biol. Transl. Sci.* **126**, 3–24 (2014).
43. K. E. Rothenberg, D. W. Scott, N. Christoforou, B. D. Hoffman, Vinculin force-sensitive dynamics at focal adhesions enable effective directed cell migration. *Biophys. J.* **114**, 1680–1694 (2018).
44. J. Schindelin *et al*., Fiji: An open-source platform for biological-image analysis. *Nat. Methods* **9**, 676–682 (2012).
45. A. Vaezi, C. Bauer, V. Vasioukhin, E. Fuchs, Actin cable dynamics and Rho/Rock orchestrate a polarized cytoskeletal architecture in the early steps of assembling a stratified epithelium. *Dev. Cell* **3**, 367–381 (2002).
46. M. Moumen *et al*., The proto-oncogene Myc is essential for mammary stem cell function. *Stem Cells* **30**, 1246–1254 (2012).
47. K. B. Deome, L. J. Faulkin, Jr, H. A. Bern, P. B. Blair, Development of mammary tumors from hyperplastic alveolar nodules transplanted into gland-free mammary fat pads of female C3H mice. *Cancer Res.* **19**, 515–520 (1959).